ACS NANO

www.acsnano.org

ARTICLE

Interface-Dependent Selectivity in Plasmon-Driven Chemical Reactions

Andrei Stefancu, Julian Gargiulo, Geoffry Laufersky, Baptiste Auguié, Vasile Chiş, Eric C. Le Ru, Min Liu, Nicolae Leopold, and Emiliano Cortés*

Cite This: *ACS Nano* 2023, 17, 3119–3127

Read Online

ACCESS | Metrics & More | Article Recommendations | Supporting Information

ABSTRACT: **Plasmonic nanoparticles can drive chemical reactions powered by sunlight. These processes involve the excitation of surface plasmon resonances (SPR) and the subsequent charge transfer to adsorbed molecular orbitals. Nonetheless, controlling the flow of energy and charge from SPR to adsorbed molecules is still difficult to predict or tune. Here, we show the crucial role of halide ions in modifying the energy landscape of a plasmon-driven chemical reaction by carefully engineering the nanoparticle−molecule interface. By doing so, the selectivity of plasmon-driven chemical reactions can be controlled, either enhancing or inhibiting the metal−molecule charge and energy transfer or by regulating the vibrational pumping rate. These results provide an elegant method for controlling the energy flow from plasmonic nanoparticles to adsorbed molecules, *in situ*, and selectively targeting chemical bonds by changing the chemical nature of the metal−molecule interface.**

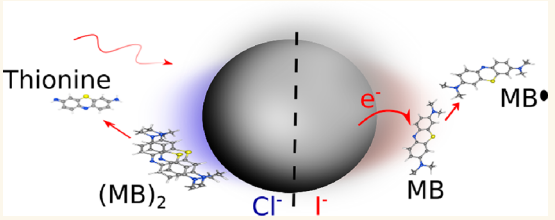

KEYWORDS: *plasmonic chemistry, halide ions, vibrational pumping, energy transfer, anti-Stokes SERS, methylene blue*

INTRODUCTION

Plasmonic nanoparticles have enabled alternative solutions for solar technologies[1] in the past decades. Their ability to capture resonantly visible light and concentrate it to the nanoscale, below the diffraction limit, mesmerized scientists and could prove useful for many critical technologies such as solar-to-chemical[2−5] and solar-to-electrical[6−8] energy conversion, (bio)sensing,[9−13] and targeted cancer treatment or imaging.[14] The fascinating properties of plasmonic nanoparticles result from the excitation of surface plasmon resonances (SPR)—the coherent oscillation of the free metal electron plasma, which couples to light and yields mixed light−matter states (plasmons) at the metal−dielectric interface.

While some applications, such as sensing, aim to design plasmonic nanostructures with minimum losses (as energetic charge carriers[15] and eventually heat) and thus maximize the plasmonic near-field enhancement (or the *Q* factor), other applications, like solar-to-chemical or solar-to-thermal energy conversion, exploit the losses of plasmonic nanostructures (i.e., energetic charge carriers). A fraction of the SPR energy is lost within a few fs by forming nonthermal electron−hole pairs (i.e., charge carriers with energy higher than the thermal energy, kT) which cause the decoherence of the plasmon resonances. After a few hundred fs, the hot carriers start to lose their energy through electron−electron collisions, forming a Fermi−Dirac distribution at an elevated temperature. After a few ps, the hot carriers lose further their energy through collisions with the phonon lattice.[3,4,16] These energetic charge carriers (hot carriers) can however be transferred to adsorbed molecular orbitals or semiconductors before they are thermalized, and drive chemical reactions. In recent years, the picture of hot carrier transfer to adsorbed molecules (i.e., plasmonic chemistry) has evolved significantly. While in the infancy of plasmonic chemistry the mechanisms and theories were mainly adapted from surface science and bulk metals, the paradigm of plasmonic chemistry has shifted toward alternative nanoscale mechanisms. The process of Landau damping, whereby a small fraction of energetic hot carriers are scattered at the nanoparticle surface and get transferred to adsorbed molecular orbitals,[17,18] has been reformulated as chemical interface damping (CID) through the seminal work of Linic et al.[19,20] and others.[21,22] As opposed to Landau damping, which is inefficient because only a small fraction of hot carriers arrives at the surface of nanostructures, in CID the hot carriers are transferred *directly* to adsorbed molecules, circumventing the competing electron−electron and electron−phonon pathways.[18,23,24] This mechanism was also postulated to explain the enhancement factor in surface enhanced Raman scattering

Received: December 6, 2022
Accepted: January 27, 2023
Published: February 1, 2023

https://doi.org/10.1021/acsnano.2c12116
ACS Nano 2023, 17, 3119−3127

(SERS) which is not entirely accounted for with the classical electromagnetic (EM) model.[25,26]

The dynamics of molecules at the surface of plasmonic nanoparticles and the chemical nature of the metal−molecule interface have been mostly overlooked in plasmonic chemistry (and not only), despite being of upmost importance in controlling the selectivity of the plasmon-driven reaction. More often than not, the energy levels and the conformation of a molecule adsorbed on plasmonic nanostructures are assumed to be the same as that of the free molecule, which is not always the case and can lead to erroneous interpretations of the experimental results. For example, the HOMO−LUMO energy gap of adsorbed molecules can shift significantly compared to the free molecule,[27] or the adsorption energy of the molecules to the metal surface can vary substantially depending on the coadsorbed species.[28−31] Moreover, the chemical nature of the metal−molecule interface (dictated by coadsorbed ions or ligands) can influence the relaxation pathways of adsorbed excited molecules and their radiative emission rates.[32] Here, by chemical nature of the metal−molecule interface, we refer to the local structure (morphological or energetic) of the metal surface at the sites where the molecule is adsorbed. On silver nanoparticles (AgNPs) for example, the local structure can be changed by coadsorbed halide ions which, owing to their strong adsorption on silver, forms surface atomic-sized AgX complexes.[32−35] Likewise, the light itself can be used to steer the selectivity of plasmon-driven chemical reactions.[36] To illustrate our current lack of understanding of molecular dynamics and interfacial effects, consider the Hofmeister effect.[37] This effect, discovered in 1888, classifies the ability of different ions to salt out or salt in proteins. Despite being observed later in other fields,[38] such as in the adsorption of ions on surfaces and electrochemical electrodes, Hofmeister series are empirical, and no satisfactory mechanism has been discovered yet.[39,40]

In this contribution we aim to further our understanding of the impact of the conformation of adsorbed molecules and of the chemical nature of the metal−molecule interface in plasmonic chemistry. Specifically, we investigate how coadsorbed halide ions at the AgNPs−methylene blue (MB) interface change the selectivity of plasmon-driven methylene blue N-demethylation to thionine. We investigate experimentally the AgNPs−MB system in two different regimes: (i) when the laser wavelength (632.8 nm) is resonantly exciting the MB molecules and (ii) when the laser wavelength (785 nm) is resonantly exciting the metal−molecule direct charge transfer (i.e., CID regime). In both cases, we find that coadsorbed halide ions (namely, AgNPs@Cl, AgNPs@Br, and AgNPs@I) dictate the flow of energy and charge from the plasmonic nanoparticles to adsorbed molecules. We demonstrate that coadsorbed Cl^- leads to the adsorption of MB in dimeric form, even at submonolayer MB concentrations, whereas coadsorbed I^- leads to the adsorption of MB in monomeric form. This difference in conformation, in turn, controls whether the MB will undergo a *demethylation reaction*, in the case of dimeric MB, or will be excited to the *triplet state* and form singlet oxygen, in the case of monomeric MB (see Figure 1). In the CID regime, we show through anti-Stokes SERS spectroscopy that I^- ions tune the metal−molecule direct charge transfer energy by upshifting the Fermi level energy of AgNPs and increase the charge transfer rate.

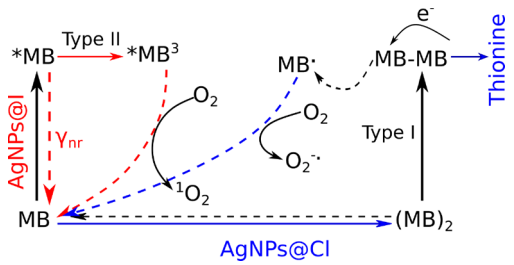

Figure 1. Pathways for methylene blue (MB) resonant photochemical reactions. For AgNPs@I (red), MB adsorbs in the monomeric form, which leads to the formation of triplet state MB ($*MB^3$), from which it can relax to the ground state through the production of singlet oxygen (type II mechanism). For AgNPs@Cl (blue), MB adsorbs as dimers, which leads to the N-demethylation of MB and formation of thionine (type I mechanism).

RESULTS

Molecular Resonance Regime (632.8 nm). First, we focus on the molecular resonance regime, when the laser wavelength falls in the absorbance band of MB. Even in the absence of plasmonic nanoparticles, the resonant MB excitation leads to photochemical reactions and the production of singlet oxygen molecules. Due to the high yield of singlet oxygen ($^1O_2$) production (~0.5), MB is a commonly used in vitro photosensitizer.[41] Photodynamic therapy for example by MB involves direct oxidation mechanisms as well as oxidation mediated by $^1O_2$, which is mainly formed through energy transfer from MB triplets to molecular oxygen.[42] Figure 1 shows the reaction pathways for resonantly photoexcited MB in the absence of plasmonic NPs (black). In addition, alternative pathways are shown for the cases where the NPs have coadsorbed halide ions such as Cl (blue) or I (red). However, this is only a simplified view, and the photoinduced effects of MB in vivo are somewhat erratic. Depending on the local environment, a cascade of chemical reactions can take place, leading to less-obvious reaction pathways and reaction products. Two major photochemical pathways are usually observed:[41,43−45] type II, where the triplet MB energy is transferred to oxygen, forming $^1O_2$, and type I where reducing agents donate an electron to MB triplets, forming the semireduced radical (MB·). In certain conditions, ground state MB itself can act as a reducing agent through the $D-{}^3D^*$ mechanism.[44] The decay of the MB· to ground state MB through O_2 in type I reactions is the most favorable way of deexcitation; however, in the absence of O_2 (for example in an N_2 atmosphere) the decay of MB· radicals can take place through less efficient pathways, leading to longer lifetimes of the MB· radicals.[41] Based on the conformation of MB (i.e., dimer or monomer), either the type I or type II photoreactions are favored. For example, in the micelle pseudophase (SDS solution), MB dimers form, which shifts the reaction pathways from a type II to a type I reaction, inhibiting the production of $^1O_2$.[41]

Figure 1 already suggests that controlling the adsorption conformation of MB (i.e., monomer or dimer) has an important outcome in the MB chemical reaction pathway. Until recently, monitoring the conformation of *adsorbed* molecules on the surface of plasmonic nanoparticles was next to impossible. The high extinction of plasmonic nanoparticles in the same EM range as the optical absorption of molecules makes it very difficult to detect the optical absorption of

https://doi.org/10.1021/acsnano.2c12116
ACS Nano 2023, 17, 3119−3127

adsorbed molecules. Surface-sensitive spectroscopy techniques, such as SERS, may provide some information, but the spectral changes are difficult to interpret and assign unambiguously to different molecular conformations. Because of this, the adsorption configuration of molecules was not considered in previous MB studies, with the implicit assumption that adsorbed MB retains the same configuration on the metal surface as in solution.

In Figure 2, we demonstrate that this assumption is not correct. We find that the adsorption of MB as monomers or

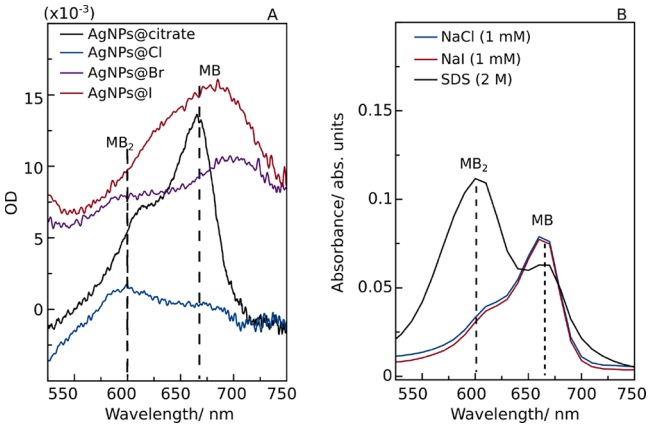

Figure 2. Absorption spectra of free and adsorbed methylene blue (MB). (A) Differential absorption spectra of MB *adsorbed* on as-synthesized AgNPs (capped by citrate), AgNPs@Cl, AgNPs@Br, and AgNPs@I at submonolayer concentration (500 nM, corresponding to approximately 0.5 MB molecules/nm^2). (B) Optical absorption of free MB with Cl$^-$, I$^-$ (the same concentration as in the SERS measurements, 1 μM) and sodium dodecyl sulfate (SDS) (/15) at a MB concentration of 50 μM. The higher MB concentration was used for SDS to favor the formation of dimeric MB and thus to allow a direct comparison with the dimeric MB differential absorption spectrum on AgNPs@Cl.

dimers can in fact be controlled through Cl$^-$ and I$^-$ ions coadsorbed on the Ag surface. We measured the optical absorption of *adsorbed* MB molecules on AgNPs@Cl, AgNPs@Br, and AgNPs@I, by using an integrating sphere spectrometer which can eliminate the strong scattering of AgNP colloids (Figure 2).[27] Cl$^-$ ions lead to the formation of MB dimers on the AgNPs surface, with a characteristic optical absorption at ~600 nm, whereas I$^-$ ions favor the adsorption of MB monomers, with the optical absorption peak at ~660 nm (Figure 2A).[46] On AgNPs@Br, both forms are present on the surface. It is important to note that this is a surface effect which does not take place in the bulk solution (i.e., MB solution without AgNPs). The broadening of the absorbance peak in the case of MB on AgNPs@I and AgNPs@Br can be explained by the inhomogeneous broadening due to varying molecule−surface interactions from one molecule to the next.[27] In the bulk MB solution, at the concentrations used in the SERS measurements (i.e., 1 μM MB and 1 mM NaCl or NaI), Cl$^-$ and I$^-$ ions do not lead to any change in the optical absorption of MB (Figure 2B). Thus, the halide ions change the ground state energy of MB dimerization on the AgNPs surface, favoring the adsorption of the monomer or dimer form. By comparison the absorption spectrum of MB at much higher concentrations in an SDS solution (Figure 2B, black spectrum) favoring the dimeric MB form shows the same features as the differential absorption spectrum of MB adsorbed on AgNPs@Cl: the peak at 600 nm is dominating the peak from monomeric MB at 660 nm. Interestingly, on as-synthesized AgNPs, capped with citrate (AgNPs@citrate) the differential MB absorption spectrum looks like the absorption spectrum of free MB in aqueous solution (Supporting Information, Figure S3), with the majority of MB in monomeric form (660 nm peak) and a small MB population in the dimeric form (600 nm shoulder). This suggests that MB does not interact with the Ag surface in the absence of halide ions, in accordance with previous studies.[30,34]

It is interesting to dwell for a moment on the significance of the results in Figure 2A. The role of charged interfaces in dye aggregation is well-known.[47] When a charged surface interacts with a dye of opposite charge, the noncovalent binding of the dye due to Coulombic forces increases the local concentration of the dye, favoring dimerization. However, in our case the results in Figure 2A are obtained for *submonolayer concentrations* of MB. This means that the formation of MB dimers or monomers on the surface of AgNPs@Cl and AgNPs@I, respectively, is not solely due to the local concentration of MB on the Ag surface. For the concentrations used in Figure 2A (see Methods), there are approximately 0.5 MB molecules/nm^2; for such intermolecular distances on the Ag surface, we would not expect a dimerization of MB molecules. Moreover, if the Coulomb attraction between MB and the negatively charged surface of AgNPs@Cl were to drive the dimerization of MB, the same should happen for AgNPs@Br and AgNPs@I, which are also negatively charged. Instead, we hypothesize that the adsorbed halide ions on the Ag surface interact specifically with MB molecules and change their dimerization constant. For example, the Br$^-$ and I$^-$ ions could interact more strongly with MB molecules and thus restrict the formation of MB dimers, whereas Cl$^-$ ions interact more weakly with the MB molecules, allowing them to diffuse on the Ag surface and form dimers. Although Cl ions have a higher charge density than Br and I (equal charge but lower radius), upon adsorption of the halide ions to the metal surface a partial charge transfer drives the reconfiguration of the surface charge density and dipole moment of the adsorbed halide ions. For example, on Pt, the adsorption of halide ions leads to a charge density build-up near the surface in the sequence Cl < Br < I. This is complemented by a change of the dipole moment of the adsorbed halide in the same sequence.[48]

The difference in the MB conformation with different coadsorbed halide ions has profound implications for plasmon-assisted chemical reactions. We illustrate this next, contrasting the two extreme cases of AgNPs@Cl (i.e., adsorbed dimer MB) and AgNPs@I (i.e., adsorbed monomer MB). In Figure 3, we show through SERS that upon resonant excitation of dimer MB adsorbed on AgNPs@Cl, thionine forms through the N-demethylation of MB (Figure 3A,B). In this case, the plasmon resonances enhance the optical absorption of the MB dimer via the local field intensity enhancement factor $|E_{Loc}/E_0|^2$. On the other hand, on AgNPs@I, no thionine was detected (Figure 3C,D), which we attribute to the MB being adsorbed in the monomer form. Instead, excited state MB is formed, which can decay back to the ground state MB or to the triplet state of MB ($^*MB^3$), which decays to the ground state MB through singlet oxygen formation (see Figure 1). The slight variation in the 480/450 cm^{-1} relative intensity in the case of AgNPs@I is due to the change in the background intensity, not to the appearance of the SERS peak at 480 cm^{-1}, specific to thionine (Figure 3C). Note that the excitation

https://doi.org/10.1021/acsnano.2c12116
ACS Nano 2023, 17, 3119−3127

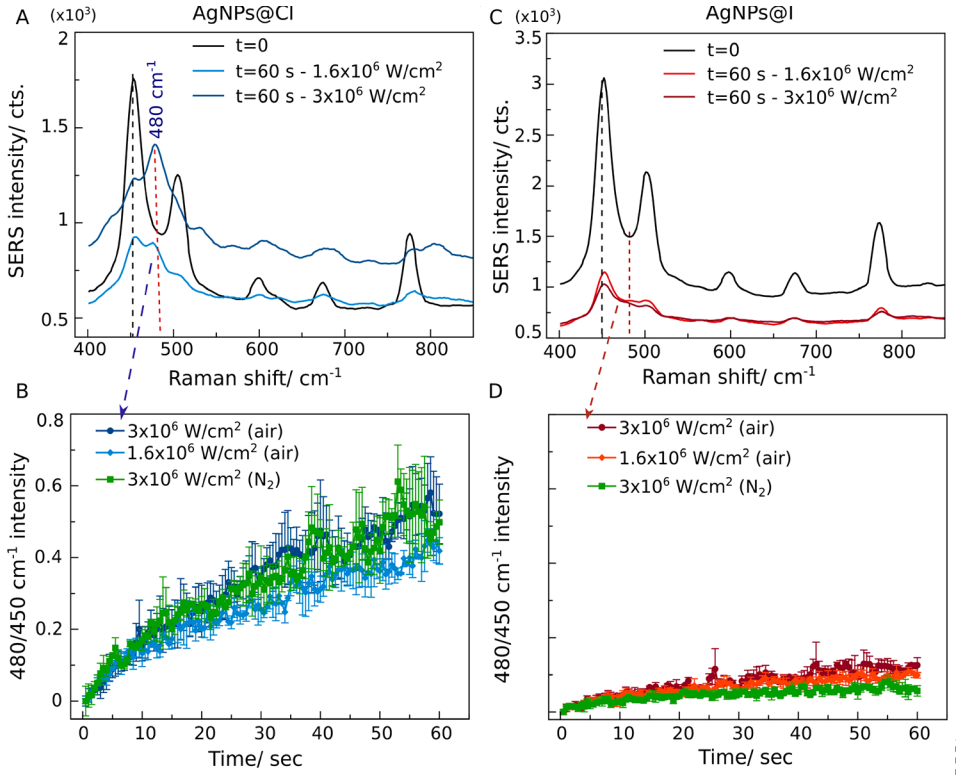

Figure 3. Interface dependent methylene blue (MB) N-demethylation to thionine. (A) Representative initial and final (after 60 s irradiation) SERS spectra of MB on AgNPs@Cl at two laser powers, showing the formation of thionine. (B) Reaction rate of N-demethylation of MB, monitored through the 480/450 cm^{-1} intensity ratio at two laser power densities, on AgNPs@Cl. (C) Representative initial and final (after 60 s irradiation) SERS spectra of MB on AgNPs@I, showing no thionine formation for both laser powers tested. (D) Reaction rate of N-demethylation of MB on AgNPs@I. The small increase of the reaction rate is due to the change in the background, not the formation of thionine. The *y*-axis scale is identical in (B) and (D) to allow for an easier comparison.

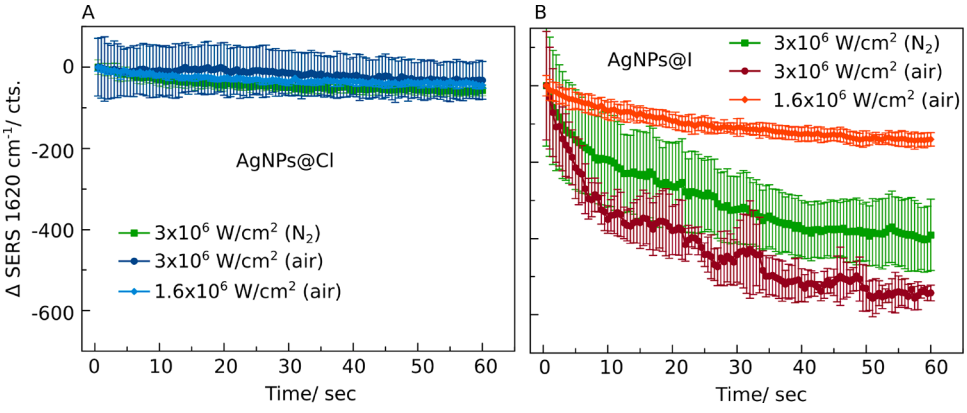

Figure 4. Photobleaching rate of MB determined through the change of the 1620 cm^{-1} SERS peak intensity, excited resonantly at 633 nm, on AgNPs@Cl (A) and AgNPs@I (B), in air and N_2. The photobleaching proceeds predominantly on monomer MB, on AgNPs@I, whereas on AgNPs@Cl the plasmonic near-fields drive the MB N-demethylation. The *y*-scale axis is identical in (A) and (B).

wavelength, 632.8 nm, is resonant with both the optical absorption of monomer and dimer MB molecules. Supporting Information Figures S4 and S5 show the calculated Raman spectra of thionine and MB dimers, respectively, proving that the 480 cm^{-1} SERS peak is indeed from thionine. The coadsorption of Cl^- and I^- ions on the surface of AgNPs was monitored, *in situ*, through their specific SERS peaks at 240 and 130 cm^{-1}, respectively (Supporting Information, Figure S6).

One interesting note is that by using a higher NA (0.8), we also observed sporadic SERS peaks from the semireduced MB radical, MB·, at 1130, 1320, and 1414 cm^{-1} besides the thionine SERS peaks (Supporting Information, Figure S7). The formation of the semireduced MB radical has been linked with the metal−MB charge transfer rather than the enhanced plasmonic near-fields.[49,50] In this case, we think that the higher excitation irradiance (of 8×10^6 W/cm^2), due to the higher NA, can drive sporadic metal−molecule charge transfer (i.e., metal−molecule charge transfer with a relatively low rate).

To gain more information on the plasmon-assisted N-demethylation of MB on AgNPs, we repeated the experiments at a power density of 3×10^6 W/cm^2, under continuous N_2

https://doi.org/10.1021/acsnano.2c12116
ACS Nano 2023, 17, 3119−3127

flow. In this case, we did not observe any significant variation in the reaction rate, suggesting that the plasmon-assisted N-demethylation of MB on AgNPs does not require the presence of oxygen. This agrees with the type I photochemical reaction of MB in the absence of AgNPs, i.e., the formation of the semireduced radical, MB·, which does not require oxygen but whose lifetime is limited by collisions with oxygen.[41]

The photobleaching rate of adsorbed MB on AgNPs@Cl and AgNPs@I, quantified through the change in the 1620 cm^{-1} SERS band intensity, further confirms the proposed mechanism. The significant decrease of the SERS intensity of MB on AgNPs@I compared to AgNPs@Cl (Figure 4) confirms that in the presence of coadsorbed I^-, the less radiative triplet MB forms (i.e., photobleaching) through intersystem crossing. Interestingly, on AgNPs@Cl, the decrease of the SERS intensity is insignificant at both laser powers tested, both in air and in N_2. This suggests that indeed dimer MB adsorbs on the AgNPs@Cl surface, which does not allow the formation of triplet state MB; instead the MB N-demethylation to thionine takes place.[41,42] On AgNPs@I on the other hand, the decrease of the SERS intensity of MB is stronger for higher excitation irradiances (Figure 4B), suggesting that with the increase in the excitation irradiance, increasingly more $*MB^3$ forms (i.e., photobleaching).[51] To further confirm this mechanism, we repeated the SERS time-series measurements under continuous flow of N_2 at the same laser power density as in air (3×10^6 W/cm^2). Under continuous N_2 flow, we found a decrease in the photobleaching rate on AgNPs@I, consistent with previous studies on the photobleaching rate of MB.[42] Although the mechanism of MB photobleaching is still debated, it has been suggested that once the excited MB goes to the triplet form through intersystem crossing, molecular oxygen could form a complex with $*MB^3$ which speeds up the photobleaching rate. In the absence of oxygen, the lifetime of the triplet MB state is longer, and light induced electron transfer between two MB molecules might promote loss of chromophore.

Chemical Interface Damping Regime (785 nm). Next, we turn our attention to the role of halide ions in controlling the dynamic (transient) AgNP−MB charge transfer at 785 nm excitation. At 785 nm excitation, the metal electrons at the Fermi level energy can be resonantly transferred to unoccupied energy states in adsorbed MB molecules. This charge transfer is not permanent, the electron being transferred back to the metal (i.e., chemical interface damping); however, this metal−molecule charge transfer can leave the MB molecules excited vibrationally, resulting in a higher anti-Stokes/Stokes SERS intensity (vibrational pumping). Vibrational pumping is physically linked to the phonon population dynamics. The Stokes process "creates" a phonon (i.e., excites vibrationally the molecule), whereas the anti-Stokes process can be viewed as the annihilation of a phonon. In most cases, the phonon population is dominated by thermal excitations. However, in cases where the laser intensity or the Stokes cross-section is enhanced (by plasmon resonances, for example), the phonons are excited at a faster rate than they relax, leading to an anomalous anti-Stokes/Stokes ratio.[52] Alternatively, phonons can be created in the adsorbed molecules through *resonant* metal−molecule charge transfer to the unoccupied molecular orbital (i.e., CID). We show here that by controlling the chemical nature of the metal−MB interface through halide ions, we can tune the CID rate and thus increase the vibrational pumping rate of MB molecules.

We show through anti-Stokes/Stokes SERS that the rate of vibrational pumping of MB almost doubles in AgNPs@I compared to AgNPs@Cl (Figure 5A,B). We believe that the

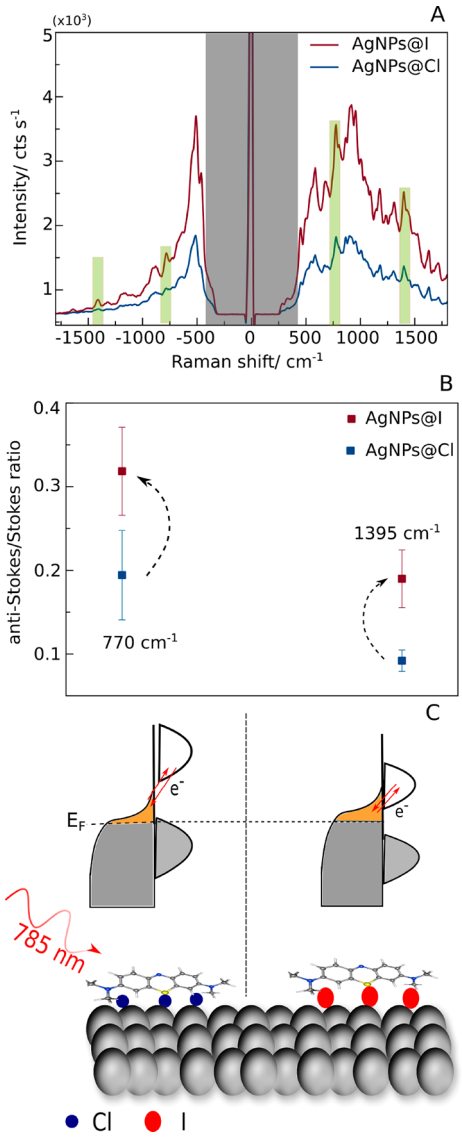

Figure 5. Shift of the AgNPs−MB energy levels dictates the direct charge transfer rate. (A) Anti-Stokes/Stokes SERS spectra of MB adsorbed on AgNPs@Cl and AgNPs@I. The gray area represents the range of the notch filter. (B) Anti-Stokes/Stokes ratio for the 770 and 1395 cm^{-1} vibrational modes of MB, showing an increased vibrational pumping rate of both modes on AgNPs@I compared to AgNPs@Cl. (C) Schematic representation of the energy levels of the AgNPs@Cl-MB and AgNPs@I-MB complexes. The upshift of Fermi level of AgNPs with coadsorbed I^- ions tunes the direct resonant metal−molecule charge transfer.

upshift of the Fermi level of the AgNPs due to adsorbed I^- ions is the main reason for the higher rate of direct metal−molecule charge transfer (i.e., CID) on AgNPs@I, which in turn yields a higher rate of vibrational pumping and anti-Stokes/Stokes ratio (Figure 5C). Surface-induced adsorbate states (as defined in the Newns−Anderson formalism[53]) can have a width of ~1 eV (for example, the $2\pi^*$ resonance state of CO on silver[24]). Thus, on AgNPs@Cl, the metal−MB direct charge transfer at 785 nm is "preresonant", where the tail of the

https://doi.org/10.1021/acsnano.2c12116
ACS Nano 2023, 17, 3119−3127

molecular acceptor state, with a low density of states, is involved in the charge transfer. By upshifting the AgNPs Fermi level through I^- ions by ~0.3 eV, the center of the molecular acceptor state of MB is involved in the metal−molecule direct charge transfer, with a higher density of states (Figure 5C). Consequently, the rate of vibrational pumping and the anti-Stokes/Stokes ratio increase by almost two times (Figure 5B). Of course, the decrease of the HOMO−LUMO energy gap of monomer MB (on AgNPs@I) compared to dimer MB (on AgNPs@Cl), from 2 to 1.87 eV, could also change the acceptor energy state of adsorbed MB. However, this energy shift of ~0.18 is smaller compared to the shift of the Fermi level energy of AgNPs@I compared to AgNPs@Cl of ~0.3 eV.[33] Because of this, we assume that the Fermi level energy shift is the main reason for the increased vibrational pumping rate of MB on AgNPs@I.

To eliminate any influence due to differences in the plasmon resonance spectrum on the silver nanowires with iodide or chloride, we acquired the anti-Stokes/Stokes SERS spectra from different locations on the silver nanowires and averaged the results. As shown in Figure 5B, the increase of the anti-Stokes/Stokes ratio is consistent throughout all acquired spectra. Moreover, all silver nanowires, with iodide or chloride, have similar plasmon resonances profiles. Thus, we do not expect that this would cause differences in the anti-Stokes/Stokes SERS ratio by enhancing more the anti-Stokes side of the MB emission on AgNPs@I compared to the MB emission on AgNPs@Cl, for example.

CONCLUSIONS

The results presented in this study highlight the crucial role played by the plasmonic metal−molecule interface in controlling the energy flow to adsorbed molecules. Particularly, for the AgNPs−MB system, coadsorbed halide ions dictate both the conformation of adsorbed MB (namely, as monomer or dimer) and the energy levels of the AgNPs−MB complex. Thus, for the resonant excitation of MB (632.8 nm), the plasmon-assisted N-demethylation of MB to thionine can proceed only when Cl^- ions are coadsorbed on AgNPs, which determine the adsorption of MB as dimers. When I^- ions are coadsorbed, MB adsorbs as monomers, and the N-demethylation reaction does not occur; instead, MB is excited to the triplet state. Even though for AgNPs@I there is enough energy provided by the plasmonic near-fields to drive the MB demethylation reaction (as for AgNPs@Cl), the reaction does not proceed because of the molecular conformation of adsorbed MB. In a different excitation regime, at 785 nm, I^- ions upshift the Fermi level energy of AgNPs and favor the direct charge transfer from the metal AgNPs to adsorbed MB (i.e., CID). This results in an increased rate of vibrational pumping of MB molecules and therefore an increased anti-Stokes/Stokes SERS ratio. These results highlight the crucial importance of controlling the energy and charge flow from plasmonic nanostructures to adsorbed molecules. We propose here that the chemical nature of the plasmonic metal−molecule interface should receive equal attention as the processes taking place inside the plasmonic structures (i.e., hot electron generation rate, light absorption, etc.) to advance our understanding of (sun)light-to-chemical energy conversion.

METHODS

Silver Nanowires Synthesis. The silver nanowires (AgNWs) were synthesized by the convective self-assembly method from citrate capped colloidal silver nanoparticles (AgNPs). AgNPs capped with citrate anions (cit-AgNPs), synthesized by Lee and Meisel method,[54] were used throughout this study. Briefly, the AgNPs were synthesized as follows: in 98 mL of ultrapure water, 17 mg of $AgNO_3$ was dissolved. The solution was boiled under constant magnetic stirring. At boiling, 2 mL of a trisodium citrate solution (1%) was added dropwise, and the solution was left to boil for another hour.

First, 2 mL of the AgNPs colloidal solution was concentrated by centrifugation at 7300*g*, for 15 min. The supernatant was discarded by pipetting, and the AgNPs were resuspended in 20 μL of ultrapure water. For all films, regular microscopy cover glasses were used as substrate, which were placed in a UV−ozone cleaner for 15 min prior to the deposition of the silver nanowires (AgNWs). The UV−ozone irradiation has a dual role: first, it cleans the coverglass from all organic impurities, and second, it turns the glass surface hydrophilic and decreases the surface tension of the colloidal AgNPs drop so that it spreads more easily in between the two glass edges. The convective self-assembly (CSA) coater comprised a motorized translational stage (Thorlabs Inc.). A cover glass that acted as a blade was fixed in the near vicinity of the substrate at the desired angle, while the concentrated AgNPs solution was placed on the substrate, underneath, and near the edge of the blade. More details about this technique can be found in previous reports.[55−57] For the deposition of the AgNW, the motorized table was programmed to move in specific sequences. First, the motorized table moves for 250 μm, at a speed of 0.05 mm/s; then, it stops for 5 s, during which the colloidal AgNPs deposit on the coverglass, forming the nanowire. This sequence was then repeated multiple times to create an optimal number of AgNW. The resulting AgNW usually had a width of ~10 μm (see Supporting Information, Figure S1). The UV−vis extinction of the colloidal AgNPs and the absorbance of the resulting AgNWs (as calculated from the reflectance spectrum $A = 1 - R$) is shown in Supporting Information, Figure S2.

SERS Measurements. For the SERS measurements on silver nanowires, the solid substrate was immersed in 2 mL of water solution containing MB (1 μM) and NaCl, NaBr, or NaI (1 mM) and left overnight at room temperature so the MB could adsorb to the Ag surface. Then, the substrate was removed from the solution, rinsed with ultrapure water, left to dry at room temperature, and placed under the microscope. SERS spectra were acquired with a Witec spectrometer, Germany, using a 20× air objective and the 633 nm wavelength provided by a He−Ne laser, with the power specified in the figures. The 785 nm wavelength for the anti-Stokes/Stokes spectra was provided by a diode laser, with a power of 2 mW. The spectra were acquired using a Nikon eclipse inverted microscope (20× air objective), coupled to a Pixies 100 BR CCD camera.

Absorption Measurements. The AgNPs, synthesized by the Lee−Meisel method, were concentrated two times (corresponding to a final concentration of 80 pM) and resuspended in ultrapure water. Next, 40 μM NaCl, NaBr, or NaI was added to the colloidal solution and left for 60 min, so the plasmon resonance stabilizes and there are no more shifts. 500 nM MB (submonolayer concentration) was added to the AgNPs@X colloidal solution, and the absorbance spectra were acquired after 10 min of incubation. The optical absorbance spectra were measured using the CloudSpec-UV instrument from Marama Labs (New Zealand). This instrument collects both extinction and absorption spectra of the sample using xenon flash lamp excitation. The absorption measurement uses an integrating sphere to remove any scattering interference from the transmission. The latter is calibrated to return the absolute absorption, with both extinction and absorption then given in units of cm^{-1}, i.e., in optical density normalized to a 1 cm path length. In order to obtain the absorption spectrum of the adsorbed MB, we subtract the absorption spectrum of AgNPs@X to that of the same solution with MB. This is called the differential absorption spectrum.[27]

https://doi.org/10.1021/acsnano.2c12116
ACS Nano 2023, 17, 3119−3127

ASSOCIATED CONTENT

Supporting Information

The Supporting Information is available free of charge at https://pubs.acs.org/doi/10.1021/acsnano.2c12116.

Optical characterization of the silver nanowires (AgNWs) used for the SERS measurements, DFT calculations of the Raman spectrum of thionine and methylene blue dimers, the SERS peaks of Ag−Cl and Ag−I stretching vibrations, and the experimental SERS peaks of thionine and semireduced methylene blue radical (PDF)

AUTHOR INFORMATION

Corresponding Author

Emiliano Cortés − *Chair in Hybrid Nanosystems, Nanoinstitute Munich, Faculty of Physics, Ludwig-Maximilians-Universität München, 80539 Munich, Germany;* orcid.org/0000-0001-8248-4165; Email: Emiliano.cortes@lmu.de

Authors

Andrei Stefancu − *Chair in Hybrid Nanosystems, Nanoinstitute Munich, Faculty of Physics, Ludwig-Maximilians-Universität München, 80539 Munich, Germany; Faculty of Physics, Babeş-Bolyai University, 400084 Cluj-Napoca, Romania;* orcid.org/0000-0002-1455-2055

Julian Gargiulo − *Chair in Hybrid Nanosystems, Nanoinstitute Munich, Faculty of Physics, Ludwig-Maximilians-Universität München, 80539 Munich, Germany;* orcid.org/0000-0002-4524-3423

Geoffry Laufersky − *The MacDiarmid Institute for Advanced Materials and Nanotechnology, School of Chemical and Physical Sciences, Victoria University of Wellington, Wellington 6140, New Zealand*

Baptiste Auguié − *The MacDiarmid Institute for Advanced Materials and Nanotechnology, School of Chemical and Physical Sciences, Victoria University of Wellington, Wellington 6140, New Zealand*

Vasile Chiş − *Faculty of Physics, Babeş-Bolyai University, 400084 Cluj-Napoca, Romania*

Eric C. Le Ru − *The MacDiarmid Institute for Advanced Materials and Nanotechnology, School of Chemical and Physical Sciences, Victoria University of Wellington, Wellington 6140, New Zealand;* orcid.org/0000-0002-3052-9947

Min Liu − *Hunan Joint International Research Center for Carbon Dioxide Resource Utilization, State Key Laboratory of Powder Metallurgy, School of Physics and Electronics, Central South University, Changsha 410083, P. R. China;* orcid.org/0000-0002-9007-4817

Nicolae Leopold − *Faculty of Physics, Babeş-Bolyai University, 400084 Cluj-Napoca, Romania;* orcid.org/0000-0002-2174-8064

Complete contact information is available at: https://pubs.acs.org/10.1021/acsnano.2c12116

Notes

The authors declare no competing financial interest.

ACKNOWLEDGMENTS

The authors acknowledge funding and support from the Deutsche Forschungsgemeinschaft (DFG, German Research Foundation) under Germanys Excellence Strategy − EXC 2089/1-390776260, the Bavarian program Solar Energies Go Hybrid (SolTech), the Center for NanoScience (CeNS), and the European Commission through the ERC Starting Grant CATALIGHT (802989). A.S. and N.L. highly acknowledge support from the Romanian Ministry of Research and Innovation, CCCDI-UEFISCDI, Project PN-III-P4-ID-PCE-2020-1292. J.G. acknowledges the support from the Humboldt Foundation.

REFERENCES

(1) Atwater, H. A.; Polman, A. Plasmonics for improved photovoltaic devices. *Nat. Mater.* **2010**, *9* (3), 205−213.

(2) Lee, J.; Mubeen, S.; Ji, X.; Stucky, G. D.; Moskovits, M. Plasmonic Photoanodes for Solar Water Splitting with Visible Light. *Nano Lett.* **2012**, *12* (9), 5014−5019.

(3) Gargiulo, J.; Berté, R.; Li, Y.; Maier, S. A.; Cortés, E. From Optical to Chemical Hot Spots in Plasmonics. *Acc. Chem. Res.* **2019**, *52* (9), 2525−2535.

(4) Cortés, E.; Besteiro, L. V.; Alabastri, A.; Baldi, A.; Tagliabue, G.; Demetriadou, A.; Narang, P. Challenges in Plasmonic Catalysis. *ACS Nano* **2020**, *14* (12), 16202−16219.

(5) Mukherjee, S.; Libisch, F.; Large, N.; Neumann, O.; Brown, L. V.; Cheng, J.; Lassiter, J. B.; Carter, E. A.; Nordlander, P.; Halas, N. J. Hot Electrons Do the Impossible: Plasmon-Induced Dissociation of H2 on Au. *Nano Lett.* **2013**, *13* (1), 240−247.

(6) Leenheer, A. J.; Narang, P.; Lewis, N. S.; Atwater, H. A. Solar energy conversion via hot electron internal photoemission in metallic nanostructures: Efficiency estimates. *J. Appl. Phys.* **2014**, *115* (13), 134301.

(7) Mubeen, S.; Lee, J.; Singh, N.; Krämer, S.; Stucky, G. D.; Moskovits, M. An autonomous photosynthetic device in which all charge carriers derive from surface plasmons. *Nat. Nanotechnol.* **2013**, *8* (4), 247−251.

(8) Nakayama, K.; Tanabe, K.; Atwater, H. A. Plasmonic nanoparticle enhanced light absorption in GaAs solar cells. *Appl. Phys. Lett.* **2008**, *93* (12), 121904.

(9) Langer, J.; Jimenez de Aberasturi, D.; Aizpurua, J.; Alvarez-Puebla, R. A.; Auguié, B.; Baumberg, J. J.; Bazan, G. C.; Bell, S. E. J.; Boisen, A.; Brolo, A. G.; Choo, J.; Cialla-May, D.; Deckert, V.; Fabris, L.; Faulds, K.; García de Abajo, F. J.; Goodacre, R.; Graham, D.; Haes, A. J.; Haynes, C. L.; Huck, C.; Itoh, T.; Käll, M.; Kneipp, J.; Kotov, N. A.; Kuang, H.; Le Ru, E. C.; Lee, H. K.; Li, J.-F.; Ling, X. Y.; Maier, S. A.; Mayerhöfer, T.; Moskovits, M.; Murakoshi, K.; Nam, J.-M.; Nie, S.; Ozaki, Y.; Pastoriza-Santos, I.; Perez-Juste, J.; Popp, J.; Pucci, A.; Reich, S.; Ren, B.; Schatz, G. C.; Shegai, T.; Schlücker, S.; Tay, L.-L.; Thomas, K. G.; Tian, Z.-Q.; Van Duyne, R. P.; Vo-Dinh, T.; Wang, Y.; Willets, K. A.; Xu, C.; Xu, H.; Xu, Y.; Yamamoto, Y. S.; Zhao, B.; Liz-Marzán, L. M. Present and Future of Surface-Enhanced Raman Scattering. *ACS Nano* **2020**, *14* (1), 28−117.

(10) Willets, K. A.; Van Duyne, R. P. Localized Surface Plasmon Resonance Spectroscopy and Sensing. *Annu. Rev. Phys. Chem.* **2007**, *58* (1), 267−297.

(11) Moisoiu, V.; Iancu, S. D.; Stefancu, A.; Moisoiu, T.; Pardini, B.; Dragomir, M. P.; Crisan, N.; Avram, L.; Crisan, D.; Andras, I.; Fodor, D.; Leopold, L. F.; Socaciu, C.; Bálint, Z.; Tomuleasa, C.; Elec, F.; Leopold, N. SERS liquid biopsy: An emerging tool for medical diagnosis. *Colloids Surf., B* **2021**, *208*, 112064.

(12) Iancu, S. D.; Cozan, R. G.; Stefancu, A.; David, M.; Moisoiu, T.; Moroz-Dubenco, C.; Bajcsi, A.; Chira, C.; Andreica, A.; Leopold, L. F.; Eniu, D.; Staicu, A.; Goidescu, I.; Socaciu, C.; Eniu, D. T.; Diosan, L.; Leopold, N. SERS liquid biopsy in breast cancer. What can we learn from SERS on serum and urine? *Spectrochimica Acta Part A: Molecular and Biomolecular Spectroscopy* **2022**, *273*, 120992.

(13) Moisoiu, T.; Dragomir, M. P.; Iancu, S. D.; Schallenberg, S.; Birolo, G.; Ferrero, G.; Burghelea, D.; Stefancu, A.; Cozan, R. G.; Licarete, E.; Allione, A.; Matullo, G.; Iacob, G.; Bálint, Z.; Badea, R. I.; Naccarati, A.; Horst, D.; Pardini, B.; Leopold, N.; Elec, F. Combined miRNA and SERS urine liquid biopsy for the point-of-care diagnosis and molecular stratification of bladder cancer. *Mol. Med.* **2022**, *28* (1), 39.
(14) Lauri, A.; Velleman, L.; Xiao, X.; Cortés, E.; Edel, J. B.; Giannini, V.; Rakovich, A.; Maier, S. A. 3D Confocal Raman Tomography to Probe Field Enhancements inside Supercluster Metamaterials. *ACS Photonics* **2017**, *4* (8), 2070−2077.
(15) Khurgin, J. B. How to deal with the loss in plasmonics and metamaterials. *Nat. Nanotechnol.* **2015**, *10* (1), 2−6.
(16) Brown, A. M.; Sundararaman, R.; Narang, P.; Goddard, W. A.; Atwater, H. A. Nonradiative Plasmon Decay and Hot Carrier Dynamics: Effects of Phonons, Surfaces, and Geometry. *ACS Nano* **2016**, *10* (1), 957−966.
(17) Govorov, A. O.; Zhang, H.; Gun'ko, Y. K. Theory of Photoinjection of Hot Plasmonic Carriers from Metal Nanostructures into Semiconductors and Surface Molecules. *J. Phys. Chem. C* **2013**, *117* (32), 16616−16631.
(18) Hartland, G. V.; Besteiro, L. V.; Johns, P.; Govorov, A. O. What's so Hot about Electrons in Metal Nanoparticles? *ACS Energy Letters* **2017**, *2* (7), 1641−1653.
(19) Boerigter, C.; Aslam, U.; Linic, S. Mechanism of Charge Transfer from Plasmonic Nanostructures to Chemically Attached Materials. *ACS Nano* **2016**, *10* (6), 6108−6115.
(20) Boerigter, C.; Campana, R.; Morabito, M.; Linic, S. Evidence and implications of direct charge excitation as the dominant mechanism in plasmon-mediated photocatalysis. *Nat. Commun.* **2016**, *7* (1), 10545.
(21) Foerster, B.; Spata, V. A.; Carter, E. A.; Sönnichsen, C.; Link, S. Plasmon damping depends on the chemical nature of the nanoparticle interface. *Sci. Adv.* **2019**, *5* (3), eaav0704.
(22) Foerster, B.; Joplin, A.; Kaefer, K.; Celiksoy, S.; Link, S.; Sönnichsen, C. Chemical Interface Damping Depends on Electrons Reaching the Surface. *ACS Nano* **2017**, *11* (3), 2886−2893.
(23) Khurgin, J. B.; Petrov, A.; Eich, M.; Uskov, A. V. Direct Plasmonic Excitation of the Hybridized Surface States in Metal Nanoparticles. *ACS Phot.* **2021**, *8* (7), 2041−2049.
(24) Persson, B. N. J. Polarizability of small spherical metal particles: influence of the matrix environment. *Surf. Sci.* **1993**, *281* (1), 153−162.
(25) Otto, A. The 'chemical' (electronic) contribution to surface-enhanced Raman scattering. *J. Raman Spectrosc.* **2005**, *36* (6−7), 497−509.
(26) Otto, A. What is observed in single molecule SERS, and why? *J. Raman Spectrosc.* **2002**, *33* (8), 593−598.
(27) Darby, B. L.; Auguié, B.; Meyer, M.; Pantoja, A. E.; Le Ru, E. C. Modified optical absorption of molecules on metallic nanoparticles at sub-monolayer coverage. *Nat. Photonics* **2016**, *10* (1), 40−45.
(28) Stefancu, A.; Nan, L.; Zhu, L.; Chiş, V.; Bald, I.; Liu, M.; Leopold, N.; Maier, S. A.; Cortes, E. Controlling Plasmonic Chemistry Pathways through Specific Ion Effects. *Adv. Opt. Mater.* **2022**, *10*, 2200397.
(29) Stefancu, A.; Iancu, S. D.; Moisoiu, V.; Leopold, N. Specific and selective sers active sites generation on silver nanoparticles by cationic and anionic adatoms. *Rom. Rep. Phys.* **2018**, *70* (4), 509.
(30) Stefancu, A.; Iancu, S. D.; Leopold, N. Selective Single Molecule SERRS of Cationic and Anionic Dyes by Cl− and Mg2+ Adions: An Old New Idea. *J. Phys. Chem. C* **2021**, *125* (23), 12802−12810.
(31) Gerold, C. T.; Henry, C. S. Observation of Dynamic Surfactant Adsorption Facilitated by Divalent Cation Bridging. *Langmuir* **2018**, *34* (4), 1550−1556.
(32) Stefancu, A.; Biro, O. M.; Todor-Boer, O.; Botiz, I.; Cortés, E.; Leopold, N. Halide−Metal Complexes at Plasmonic Interfaces Create New Decay Pathways for Plasmons and Excited Molecules. *ACS Photonics* **2022**, *9* (3), 895−904.
(33) Stefancu, A.; Lee, S.; Zhu, L.; Liu, M.; Lucacel, R. C.; Cortés, E.; Leopold, N. Fermi Level Equilibration at the Metal−Molecule Interface in Plasmonic Systems. *Nano Lett.* **2021**, *21* (15), 6592−6599.
(34) Leopold, N.; Stefancu, A.; Herman, K.; Tódor, I. S.; Iancu, S. D.; Moisoiu, V.; Leopold, L. F. The role of adatoms in chloride-activated colloidal silver nanoparticles for surface-enhanced Raman scattering enhancement. *Beilstein J. Nanotechnol.* **2018**, *9*, 2236−2247.
(35) Zhang, Y.; Prabakar, S.; Le Ru, E. C. Coadsorbed Species with Halide Ligands on Silver Nanoparticles with Different Binding Affinities. *J. Phys. Chem. C* **2022**, *126* (20), 8692−8702.
(36) Peiris, E.; Hanauer, S.; Le, T.; Wang, J.; Salavati-fard, T.; Brasseur, P.; Formo, E. V.; Wang, B.; Camargo, P. Controlling Selectivity in Plasmonic Catalysis: Switching Reaction Pathway from Hydrogenation to Homocoupling Under Visible Light Irradiation. *Angew. Chem., Int. Ed.* **2022**, *62*, e202216398.
(37) Hofmeister, F. Zur Lehre von der Wirkung der Salze. *Archiv für experimentelle Pathologie und Pharmakologie* **1888**, *24* (4), 247−260.
(38) Oncsik, T.; Trefalt, G.; Borkovec, M.; Szilagyi, I. Specific Ion Effects on Particle Aggregation Induced by Monovalent Salts within the Hofmeister Series. *Langmuir* **2015**, *31* (13), 3799−3807.
(39) Ninham, B. W.; Duignan, T. T.; Parsons, D. F. Approaches to hydration, old and new: Insights through Hofmeister effects. *Curr. Opin. Colloid Interface Sci.* **2011**, *16* (6), 612−617.
(40) Parsons, D. F.; Boström, M.; Maceina, T. J.; Salis, A.; Ninham, B. W. Why Direct or Reversed Hofmeister Series? Interplay of Hydration, Non-electrostatic Potentials, and Ion Size. *Langmuir* **2010**, *26* (5), 3323−3328.
(41) Junqueira, H. C.; Severino, D.; Dias, L. G.; Gugliotti, M. S.; Baptista, M. S. Modulation of methylene blue photochemical properties based on adsorption at aqueous micelle interfaces. *Phys. Chem. Chem. Phys.* **2002**, *4* (11), 2320−2328.
(42) Nassar, S. J. M.; Wills, C.; Harriman, A. Inhibition of the Photobleaching of Methylene Blue by Association with Urea. *ChemPhotoChem* **2019**, *3* (10), 1042−1049.
(43) Nemoto, M.; Usui, Y.; Koizumi, M. The Occurrence of a D−D Mechanism in the Ethanol Solution of Eosine. *Bull. Chem. Soc. Jpn.* **1967**, *40* (5), 1035−1040.
(44) Kosui, N.; Uchida, K.; Koizumi, M. The Switch-over from the D−R to the D−D Mechanism in the Photoreduction of Methylene Blue. *Bull. Chem. Soc. Jpn.* **1965**, *38* (11), 1958−1965.
(45) Ravanat, J.-L.; Cadet, J.; Araki, K.; Toma, H. E.; Medeiros, M. H. G.; Mascio, P. D. Supramolecular Cationic Tetraruthenated Porphyrin and Light-Induced Decomposition of 2-Deoxyguanosine Predominantly Via a Singlet Oxygen-Mediated Mechanism. *Photochem. Photobiol.* **1998**, *68* (5), 698−702.
(46) Wang, J.; Lin, C.-Y.; Moore, C.; Jhunjhunwala, A.; Jokerst, J. V. Switchable Photoacoustic Intensity of Methylene Blue via Sodium Dodecyl Sulfate Micellization. *Langmuir* **2018**, *34* (1), 359−365.
(47) Severino, D.; Junqueira, H. C.; Gugliotti, M.; Gabrielli, D. S.; Baptista, M. S. Influence of Negatively Charged Interfaces on the Ground and Excited State Properties of Methylene Blue ¶. *Photochem. Photobiol.* **2003**, *77* (5), 459−468.
(48) Gossenberger, F.; Roman, T.; Forster-Tonigold, K.; Groß, A. Change of the work function of platinum electrodes induced by halide adsorption. *Beilstein Journal of Nanotechnology* **2014**, *5*, 152−161.
(49) Oksenberg, E.; Shlesinger, I.; Xomalis, A.; Baldi, A.; Baumberg, J. J.; Koenderink, A. F.; Garnett, E. C. Energy-resolved plasmonic chemistry in individual nanoreactors. *Nat. Nanotechnol.* **2021**, *16*, 1378−1385.
(50) Rao, V. G.; Aslam, U.; Linic, S. Chemical Requirement for Extracting Energetic Charge Carriers from Plasmonic Metal Nanoparticles to Perform Electron-Transfer Reactions. *J. Am. Chem. Soc.* **2019**, *141* (1), 643−647.
(51) Etchegoin, P. G.; Lacharmoise, P. D.; Le Ru, E. C. Influence of Photostability on Single-Molecule Surface Enhanced Raman Scattering Enhancement Factors. *Anal. Chem.* **2009**, *81* (2), 682−688.

https://doi.org/10.1021/acsnano.2c12116
ACS Nano 2023, 17, 3119−3127

(52) Maher, R. C.; Galloway, C. M.; Le Ru, E. C.; Cohen, L. F.; Etchegoin, P. G. Vibrational pumping in surface enhanced Raman scattering (SERS). *Chem. Soc. Rev.* **2008**, *37* (5), 965−979.
(53) Newns, D. M. Self-Consistent Model of Hydrogen Chemisorption. *Phys. Rev.* **1969**, *178* (3), 1123−1135.
(54) Lee, P. C.; Meisel, D. Adsorption and surface-enhanced Raman of dyes on silver and gold sols. *J. Phys. Chem.* **1982**, *86* (17), 3391−3395.
(55) Farcau, C.; Sangeetha, N. M.; Moreira, H.; Viallet, B.; Grisolia, J.; Ciuculescu-Pradines, D.; Ressier, L. High-Sensitivity Strain Gauge Based on a Single Wire of Gold Nanoparticles Fabricated by Stop-and-Go Convective Self-Assembly. *ACS Nano* **2011**, *5* (9), 7137−7143.
(56) Flauraud, V.; Mastrangeli, M.; Bernasconi, G. D.; Butet, J.; Alexander, D. T. L.; Shahrabi, E.; Martin, O. J. F.; Brugger, J. Nanoscale topographical control of capillary assembly of nanoparticles. *Nat. Nanotechnol.* **2017**, *12* (1), 73−80.
(57) Botiz, I.; Codescu, M.-A.; Farcau, C.; Leordean, C.; Astilean, S.; Silva, C.; Stingelin, N. Convective self-assembly of π-conjugated oligomers and polymers. *Journal of Materials Chemistry C* **2017**, *5* (10), 2513−2518.

https://doi.org/10.1021/acsnano.2c12116
ACS Nano 2023, 17, 3119−3127